京都大学防災研究所年報　第51号B　平成 20 年 6 月
Annuals of Disas. Prev. Res. Inst., Kyoto Univ., No. 51 B, 2008

Assessment of Prediction Uncertainty under Scale-dependant Condition of Rainfall-Runoff Modeling

Giha LEE*, Yasuto TACHIKAWA* and Kaoru TAKARA

*Graduate school of Urban and Environment Engineering, Kyoto University

Synopsis

This paper aims at investigating prediction uncertainty due to parameter and input under scale-dependant condition of rainfall-runoff modeling. Moreover, a new rainfall-runoff modeling framework considering uncertainty components involved in modeling processes is proposed to provide guideline for future modeling direction. First, parameter compatibility is evaluated in order to search for the suitable resolution of DEM, which provides better model performance and less simulation error but represent natural heterogeneity appropriately. Second, scenario-based applications are performed to examine the effect of input uncertainty due to spatial variability of rainfall data on model predictions. Finally, three guideline indices with respect to model performance, model structural stability and parameter identifiability are proposed to explain limitations of a conventional modeling protocol and then a new modeling framework is outlined by incorporating these indices into the model evaluation procedure.

Keywords: prediction uncertainty, parameter compatibility, spatial variability of rainfall, new modeling framework

1. Introduction

Uncertainty is an integral part of not only hydrological modeling but decision making of water management policy since, for example, a stochastic model like random field generator is used to interpolate rainfall over space and time and these data are inputs into a rainfall-runoff model for computing water levels or discharges at specific locations that in turn are used as inputs to an ecological model and finally, the outputs from ecologic models can be input to an integrated water management model. It is therefore crucial to identify sources of uncertainty for protecting their propagation into output variables (Wagener and Gupta, 2005). A good discussion of these sources of uncertainty can be found in Melching (1995) and Gupta *et al.* (2003). They classified the uncertainty in the hydrological modeling process into three major components; model structural uncertainty, parameter uncertainty and data uncertainty.

Here, data uncertainty is errors introduced by the measurement, by the temporal and spatial discretization of measurements or by data processing. Model structure uncertainty is interpreted as simplifications and/or inadequacies in the description of real natural systems. Parameter uncertainty is due to multiple regions of attraction in model space and multiple local optima within those regions, which make it difficult to identify the globally-optimum model. Besides these well known uncertainty components, many other components such as imperfect initial conditions, natural randomness and so on are also included in hydrological modeling.

In the context to uncertainty assessment, this paper attempts to account for the influence of two main sources, parameter and input error on model predictions. In addition, the effect of topographic scale on prediction uncertainty assessment procedure is also

presented. Finally, we propose an extended rainfall-runoff modeling framework under uncertainty by incorporating two conditioning processes into modeling processes. First, a set of model structures (from simple bucket model to scale-dependant complex models) is evaluated multi-dimensionally with respect to model performance, model structural stability and parameter identifiability. Note that all of evaluative indices are derived on the basis of the author's previous papers including Lee *et al.* (2006, 2007, 2008). Second, complementary data is imposed on the conditioned model space, given from the first stage for either further rejecting unreliable parameter set(s) or confirming reliable parameter one(s). In this study, spatiotemporal internal responses of catchment (Sayama *et al.*, 2007) is utilized as complementary constraints to filter out a non-physical parameter set among various plausible ones within high dimensional parameter space of a distributed rainfall-runoff model.

Section 2 introduces basic materials for objectives of this study, that is, study site, used data and models and section 3 presents the analysis of parameter compatibility under scale-dependant condition of distributed rainfall- runoff modeling. The propagation of input uncertainty due to spatial variability of rainfall field into model prediction is dealt in section 4. Section 5 addresses the extended rainfall-runoff modeling framework under uncertainty and suitability of the newly developed framework is verified by a case study. Finally, we conclude the paper with summaries in Section 6.

2. Materials

2.1 Hydrologic models

Three different model structures are built under OHyMoS for purposes of each specific application.

2.1.1 Storage Function Method (SFM)

This model is a simple nonlinear reservoir model and it is still widely used in practical engineering works in Japan despite its simplicity. The form of SFM is expressed as:

$$\frac{dS}{dt} = r_e(t - T_l) - q, \qquad S = kq^p \tag{1}$$

$$r_e = \begin{cases} f \times r, & if \quad \sum r \le R_{SA} \\ r, & if \quad \sum r > R_{SA} \end{cases} \tag{2}$$

where S is water storage; r_e is effective rainfall intensity; r is rainfall intensity; q is runoff; t is time; k is storage coefficient; p is coefficient of nonlinearity; f is primary runoff ratio; T_l is lag time and R_{SA} is accumulated saturated rainfall. There are four parameters (k, p, f and R_{SA}) to be optimized in SFM.

2.1.2 Kinematic Wave Method for Subsurface and Surface runoff with Single Threshold (KWMSS1)

In this model, the catchment surface is assumed to be covered with a highly permeable stratum entitled 'A-layer', having uniform thickness, D within pre-defined computational building blocks (*e.g.*, grid cell, sub-catchment). A depth, d is referred to as a threshold to take into account the surface flow and subsurface flow and it is defined as $d = D\gamma$, where γ is the porosity of the A-layer (see Figure 1(a)). Takasao and Shiiba (1988) proposed the following piecewise relation between water depth, h and discharge per unit width, q.

$$q = \begin{cases} vh, & 0 \le h \le d \\ vh + \alpha(h-d)^m, & d < h \end{cases} \tag{3}$$

where $v = k_d i$; $\alpha = \sqrt{i}/n$; v is velocity through A-layer; i is slope gradient; k_d is saturated hydraulic conductivity; n is Manning's roughness coefficient and

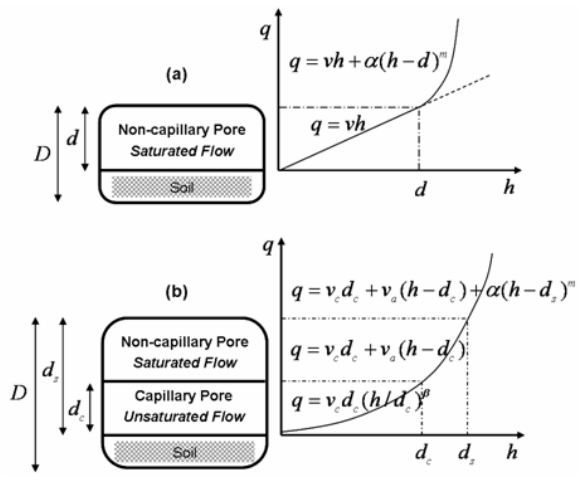

Fig. 1 Schematic model structures for (a) KWMSS1 and (b) KWMSS2.

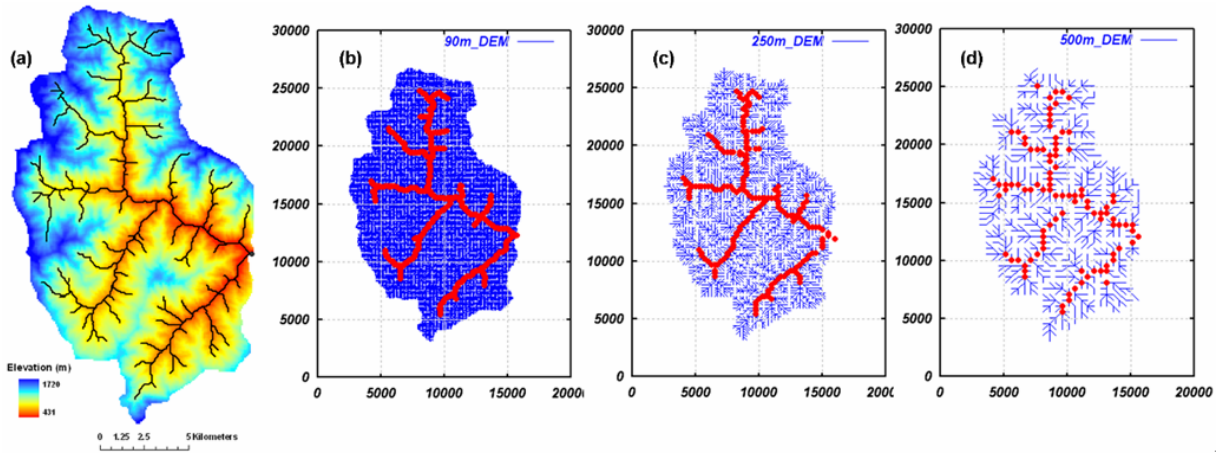

Fig. 2 The study site; (a) elevation map and (b) ~ (d) Drainage networks of 90m, 250m and 500m DEMs built with a set of slope elements (solid line) and river nodes (circle).

if the overland flow follows Manning's resistance law, m=5/3. Three model parameters (n, k_d and d) require to be adjusted against observed data.

2.1.3 Kinematic Wave Method for Subsurface and Surface runoff with Double Thresholds (KWMSS2)

The KWMSS2 assumes that a permeable soil layer covers the hillslope as shown in Figure 1(b). The soil layer consists of a capillary layer in which unsaturated flow occurs and a non-capillary layer where saturated flow occurs. According to this runoff mechanism, if the depth of water, h is higher than the soil depth, D, then overland flow occurs (Tachikawa *et al.*, 2004). The stage-discharge relationship is defined as:

$$q=\begin{cases} v_c d_c (h/d_c)^{\beta}, & 0 \le h \le d_c \\ v_c d_c + v_a (h-d_c), & d_c \le h \le d_s \\ v_c d_c + v_a (h-d_c) + \alpha (h-d_s)^m, & d_s \le h \end{cases} \quad (4)$$

$$\frac{\partial h}{\partial t} + \frac{\partial q}{\partial x} = r(t) \quad (5)$$

Flow rate of each slope segment is calculated by governing equations (Eq.s(3) and (4)) combined with the continuity equation (Eq.(5)), where $v_c = k_c i$; $v_a = k_a i$; $k_c = k_a / \beta$; $\alpha = \sqrt{i}/n$; i is slope gradient; k_c is hydraulic conductivity of the capillary soil layer; k_a is hydraulic conductivity of the non-capillary soil layer; n is roughness coefficient; the water depth corresponding to the water content is d_s and the water depth corresponding to maximum water content in the capillary pore is d_c. Detailed explanations of the model structure appear in Tachikawa *et al.* (2004). There are five parameters (n, k_a, d_s, d_c and β), which are assumed to be spatially-homogeneous, to be optimized in KWMSS2.

2.2 Study site and historical data

The study site is the Kamishiiba catchment, upstream area of the Kamishiiba dam, which lies within Kyushu region in Japan and covers area of 211km^2. The topography of this area is hilly with the elevation varying from 431m to 1720m and most of land use type is forest. The observed discharge data converted from water level of dam inflow having 10min temporal resolution is available (Kyushu Electric Co., Inc.). Operational radar rainfall data observed from Ejiroyama X-band radar covering a radius of 128km are available for this study area. The rainfall field contains 10min temporal and 1km spatial resolutions.

2.3 Delineation of drainage networks for five different DEMs

Distributed rainfall-runoff modeling usually relies on topography, land use and soil property for both overland flow and sub-surface flow. In general, the drainage network is derived by connecting each grid within study domain of interest and this drainage network controls the rate at which runoff is routed to the downstream outlet. In this study, the Kamishiiba catchment is represented by a set of slope elements and river nodes. Figures 2(b) ~ (d) illustrate the examples

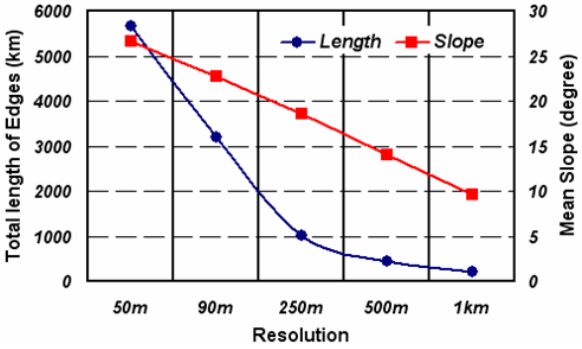

Fig. 3 Resolution effect on topographic characteristics of the study area.

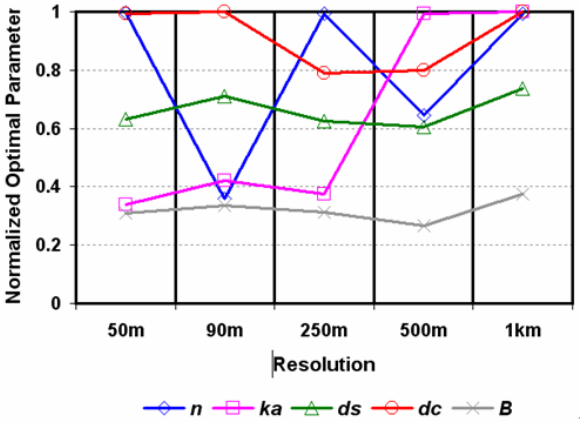

Fig. 4 Normalized optimal parameter sets of each resolution.

of drainage networks for 90m, 250m and 500m DEMs, respectively. The drainage network with the fine resolution (*e.g.*, 90m) is much denser than the one based on the coarse resolution (*e.g.*, 500m).

Figure 3 clearly shows that the grid cell resolution profoundly affects the topographically-based distributed rainfall-runoff model. Total length of the drainage networks is shortened and mean slope of the catchment is flattened as the spatial resolution becomes coarser. Mean slope varies mildly while drainage network length is changed drastically according to the spatial resolution but a more dominant factor into the runoff simulation is still unknown since both characteristics affects a hydrological response in combination. Nevertheless, it is true that this topographic variation due to the spatial resolution of DEM directly influences catchment responses (Vieux, 1993). It means that shorter drainage length reduces the lag time of water through the catchment while steeper slopes accelerates the arrival time of water to the outlet.

3. Parameter Compatibility under Scale-dependant Condition

3.1 Model calibration and resolution effect on parameter

Shuffled Complex Evolution (SCE; Duan *et al.*, 1992), computer-based single-objective automatic optimization algorithm, is used for calibration of KWMSS2 with an objective function, Simple Least Square (SLS), defined as:

$$\mathrm{SLS} = \sum_{t=1}^{N} (q_t^{obs} - q_t(\theta))^2 \qquad (6)$$

where q_t^{obs} is observed streamflow value at time t; $q_t(\theta)$ is simulated streamflow value at time t using a parameter set θ and N is the number of flow values available.

Calibrated parameter sets of each resolution are plotted in Figure 4, as a normalized form. Normalized parameter sets indicate that spatial resolution affects the model calibration significantly. That is, different topographic characteristic controlling runoff processes over the catchment, needs different parameter sets for best matching to the observed hydrograph. Indeed, parameters, d_s and β are relatively constant but the other parameters are very much fluctuated irregularly according to the resolution. All models using the calibrated model parameters lead to very good model performances regardless of DEM size while calibration time of the finest resolution is far slower than the coarsest resolution. It can be seen that modelers don't need to insist on the model based on fine resolutions in practical rainfall-runoff modeling for streamflow estimation. However, if the resolution is too coarse, important variation in space will be missed and it will cause inaccurate model results. On the other hand, over-sampling at too fine resolution deteriorates computer efficiency and causes the model to run more slowly. Therefore, the ideal in distributed rainfall-runoff modeling is to find the resolution that adequately samples the data for the simulation yet is not so fine that computational burden results. In this regard, parameter compatibility is assessed to test transferability of tuned parameter of each resolution to different resolutions.

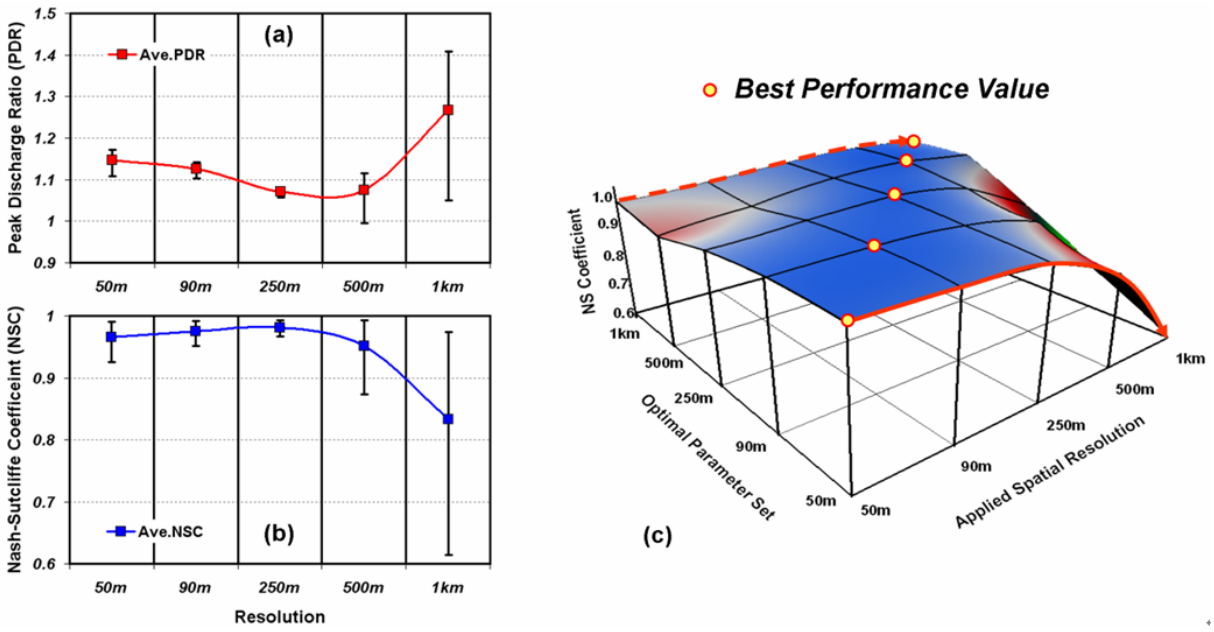

Fig. 5 Computed assessment indices of parameter compatibility; (a) Peak Discharge Ratio (PDR), (b) Nash-Sutcliffe Coefficient (NSC) and (c) 3-D plot of NSC.

3.2 Assessment of parameter compatibility

Parameter compatibility is evaluated by two indices, Peak Discharge Ratio (PDR) and Nash-Sutcliffe Coefficient (NSC), expressed as:

$$\mathrm{PDR} = q_{sim}^{peak} / q_{obs}^{peak} \tag{7}$$

$$\mathrm{NSC} = 1 - \frac{\sum_{t=1}^{N} (q_t^{obs} - q_t(\theta))^2}{\sum_{t=1}^{N} (q_t^{obs} - q^{mean})^2} \tag{8}$$

where q_{sim}^{peak} is simulated peak discharge and q_{obs}^{peak} is observed peak discharge. The PDR measures tendency of the simulated peak discharge to be larger or smaller than the observed peak discharge. The NSC measures a relative magnitude of the residual variance to the variance of the observed stream flows and the optimal value of both measures is 1.0.

Figures 5(a) and 5(b) present the computed PDRs and NSCs, respectively for all applications. Squares in the plots indicate average values of two indices and vertical lines indicate the boundary for maximum and minimum values of two indices. Figure 5(c) is the three dimensional plot of NSCs to show the parameter compatibility in an easy-to-understand manner.

The assessment results shows that all model performances with optimal parameter sets are good (NSC > 0.95, see the circles in Figure 5(c)) and the optimal parameter sets based on coarser DEMs are well applicable for hydrograph simulations for finer resolution based models while contrary applications gives very poor model performances (*i.e.*, both the boundaries and the average values of two indices for finer resolutions are very narrower and better than those for coarser resolutions). Indeed, PDR of the coarsest resolution is much over-estimated and also NSC value is much under-estimated when comparing to the 250m DEM showing the best parameter compatibility. There are two interesting findings. First, if the resolution which is based on model calibration is coarser than the resolution to be transferred, parameter compatibility is good while the contrary applications lead to worse parameter compatibility. For example, the best-performing parameter set of 50m resolution tends to be less transferable as the applied resolution becomes coarser from 50m to 1km (see solid arrow in Figure 5(c)) while the optimal one of 1km is well applicable for all resolutions (see dashed arrow in Figure 5(c)). Second, the model with the finest resolution, 50m does not guarantee the best parameter compatibility. Instead, 250m-based model gives stable model performances regardless of parameter sets given

different DEMs (see Figures 5(a) and (b)). In spite of different parameter values, they can lead to practically identical measures (*e.g.*, NSC) of model performance. Beven and Binley (1992) used the special term 'equifinality' to define this hydrological phenomenon. In the context of equifinaility problem, a complex drainage network has higher potential causing equifinality problem than a simple drainage network derived from large spatial resolutions.

4. Input Uncertainty due to Spatial Variablity of Rainfall and Their Effect on Runoff Simulation

4.1 Rainfall Scenarios

Radar rainfall fields of two historical flood events by Typhoon No. 9, 1997 (Event 1) and No. 7, 1999 (Event 2) are obtained from the Ejiroyama radar station. However, there are no ground raingauge stations within the study catchment. For various rainfall scenarios, five grid cells are selected from observed radar fields and then we assume these cells as virtual gauge stations representing downstream (gauge 1), mid-stream (gauge 2) and upstream (gauges 3, 4 and 5) in the Kamishiiba catchment. Six rainfall fields are generated based on the chosen virtual stations using Nearest Neighborhood Interpolation (NNI) method in the order of number of gauges used in interpolation; from scenario 2 to scenario 7. Moreover, raingauges of scenario 6 are rearranged randomly to examine the effect of spatial arrangement of raingauges on runoff simulations. Scenario 7 indicates this rearranged rainfall field. Scenario 8 is the 180° rotated original radar data in order to investigate more clearly the influence of the rainfall spatial pattern due to relocation of rainfall cells, on catchment responses. KWMSS2 is calibrated by the scenario1-based rainfall data of two events and the rainfall of scenario 1 is assumed to provide the best estimate of input to the model.

Figures 6(a) and 7(a) describe the spatial distributions of the total rainfall depths of two events for all rainfall scenarios used in this study. Moreover, Figures 6(b) and 7(b) show the areal mean rainfall sequences of each rainfall scenario under 250m DEM; the blue thick solid line is the original radar rainfall data (*i.e.,* scenario 1) and other lines are the rainfall time series of other different scenarios. For each rainfall scenario, the relative errors in rainfall and catchment responses are computed and summarized in subsequent subsection.

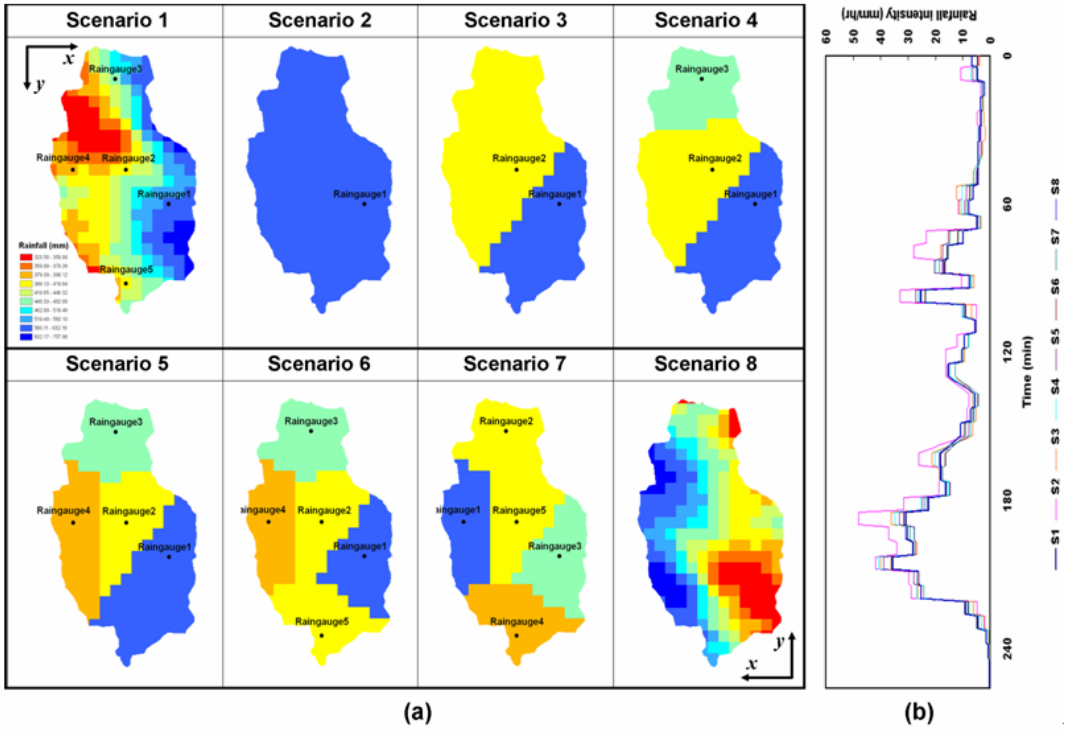

Fig. 6 (a) Spatial patterns of accumulated rainfall and (b) time series of areal mean rainfall for all rainfall scenarios of Event1.

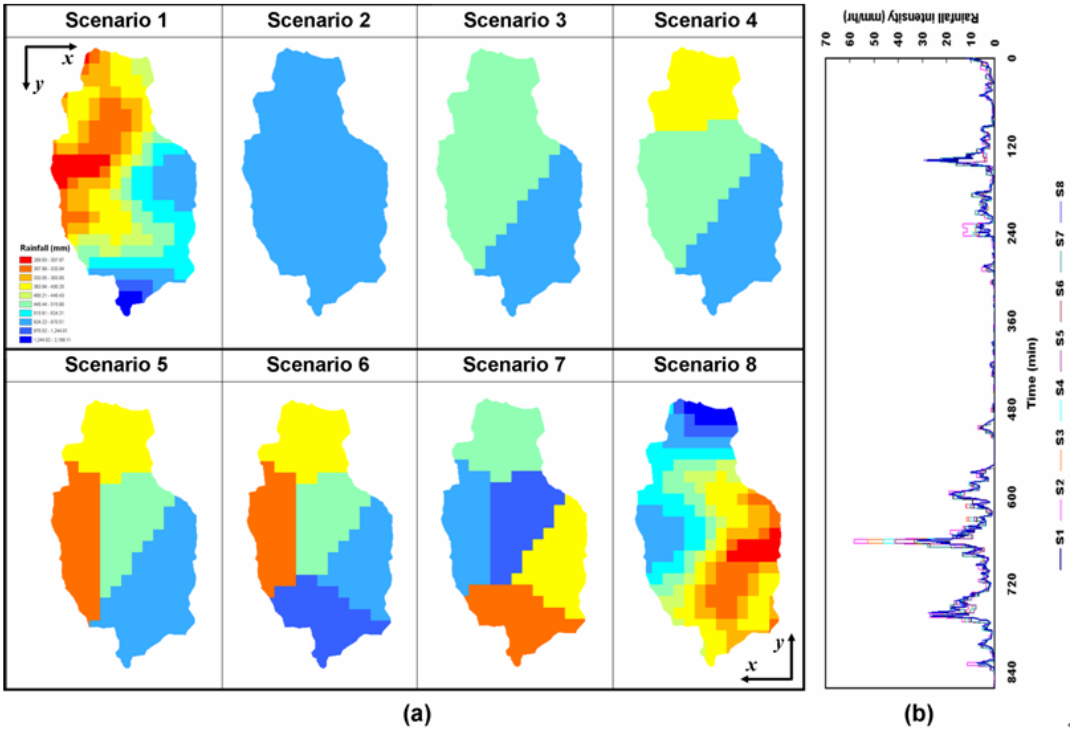

Fig. 7 (a) Spatial patterns of accumulated rainfall and (b) time series of areal mean rainfall for all rainfall scenarios of Event 2.

4.2 Effect of Input Uncertainty on Runoff Volume, Peak Flow and Time of Peak flow

The relative error of rainfall and runoff simulation is computed as:

$$\frac{R_{S_1} - R_{S_i}}{R_{S_1}} \times 100 \qquad i = 2, \cdots\cdots, 8 \tag{9}$$

where R_{S_1} is either the accumulated areal rainfall or the general properties of runoff such as runoff volume, peak flow and timing of peak based on input of scenario 1 and R_{S_i} is the variable of interest in scenario *i*. The relative error of rainfall to all rainfall patterns is illustrated in Figure 8. Figure 8(a) clearly shows that the most spatially uniform rainfall fields fail to estimate accurate amounts of areal rainfall for both events. Regardless of DEM sizes the rainfall of scenario 2 is overestimated approximately 25% for Event 1 and 32% for Event 2, respectively. However, more spatially distributed rainfall pattern does not yield more accurate areal rainfall in this catchment. All scenarios except for scenario 2 do not exceed the relative error of ±5% in Event 1 while errors of scenario 6 and 7 in Event 2 are much larger even if their spatial patterns are more heterogeneous than scenarios 3, 4 and 5. The reason is that the values of rainfall of raingauge 4 at each time step are much higher than those of the other raingauges so that total amounts of rainfall in the cases including raingauge 4 are computed highly. Figure 8 supports that all of areal rainfall depths across the catchment and error patterns for each scenario are identical without regard of DEM sizes because of similar contributing areas in spite of different topographic resolutions.

The relative error of prediction according to the rainfall scenarios is summarized in Figure 9. The computed results present that total amount of rainfall and temporal variability of rainfall during storm events affect more significantly runoff simulation than the spatial pattern itself of rainfall in the study catchment. Previous researches also highlighted the importance of estimating global volume of rainfall input for prediction of hydrographs (Beven and Hornberger, 1982; Obled *et al*., 1994). The difference of rainfall volume due to raingauge sampling results in very similar error patterns with respect to runoff volume and peak discharge while peak time error is less sensitive to the spatial pattern according to rainfall scenarios.

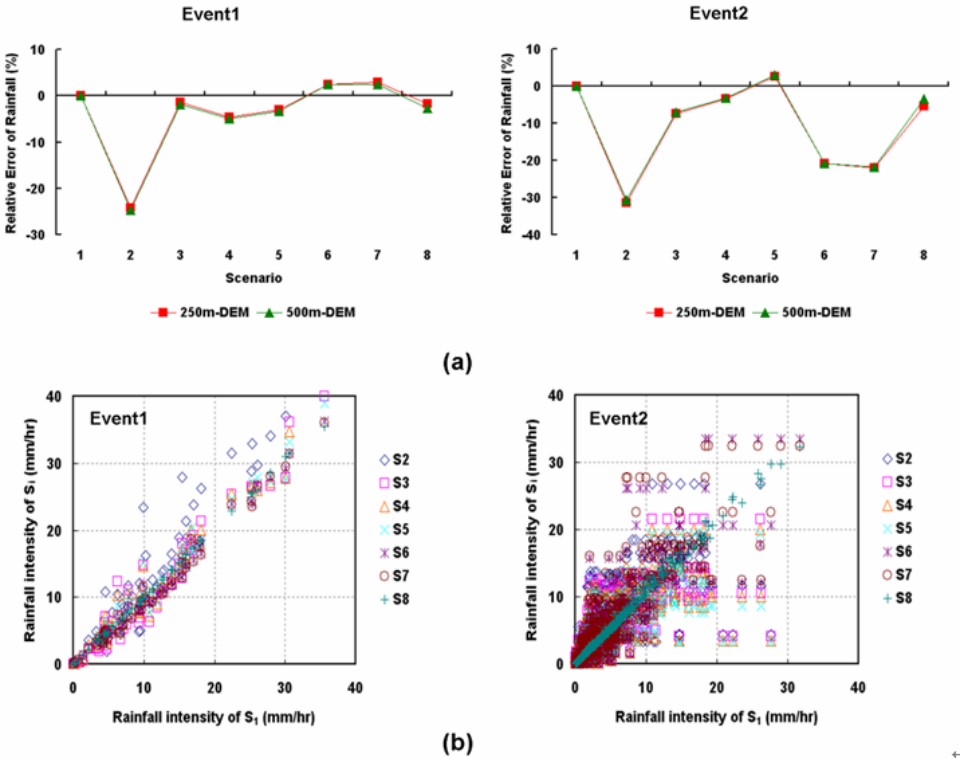

Fig. 8 (a) Relative error of rainfall for 8 scenarios and (b) comparison of rainfall derived from each scenario under 250m DEM (S_1 and S_i indicate scenario 1 and scenario i respectively, i=2,…,8)

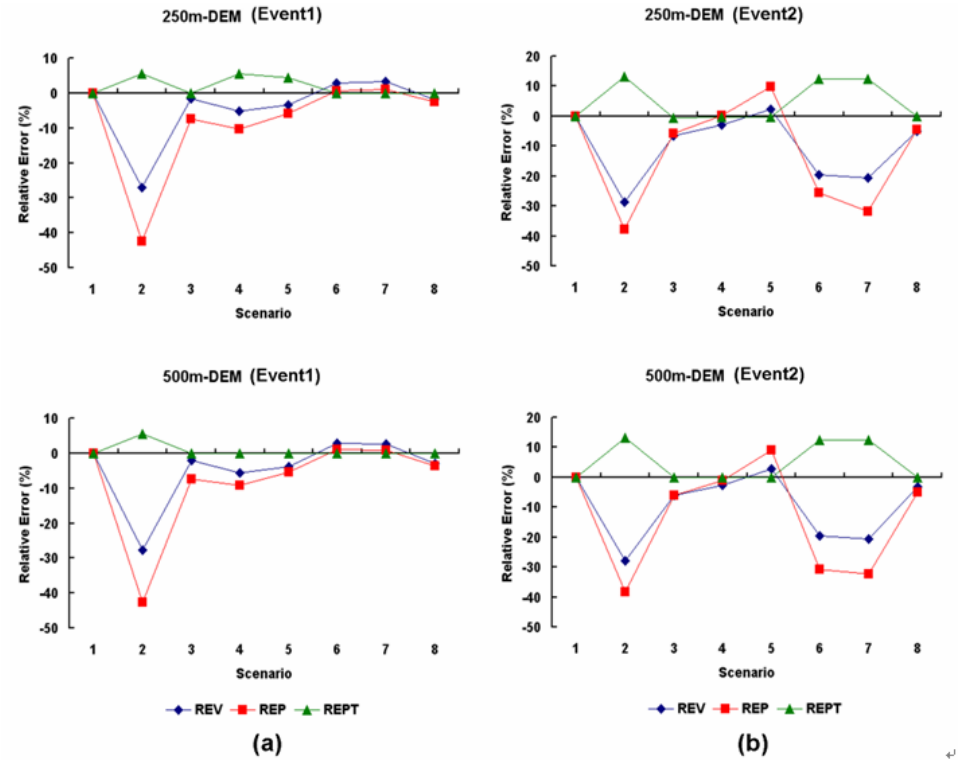

Fig. 9 Effect of rainfall error to catchment responses for all of 8 scenarios; (a) the results of Event 1 and (b) the results of Event 2 (REV, REP and REPT indicate relative error of runoff volume, relative error of peak discharge and relative error of peak time, respectively).

Even peak times of scenario 2 in Event 1 and scenario 2, 6 and 7 in Event 2 show the relative error less than 12% while the errors in terms of runoff volume and peak flow for these scenarios are much deviated from original data of scenario 1. Propagation of rainfall error to the general properties of runoff does not show significant difference between two DEM sizes. From these results, it is important to note that spatially less distributed rainfall data can satisfy rainfall-runoff simulations regardless of the level of its spatial heterogeneity in this small mountainous catchment if the interpolated rainfall fields by a few raingauges capture a similar global volume of rainfall input during specific event periods. Therefore, it is not surprising that a practitioner often prefers a parsimonious model with uniform rainfall input to a complex distributed model with non-uniform input if his objective is just streamflow forecasting because well-calibrated lumped runoff models also produces good simulated results (Franks *et al*., 2006). However, it does not imply that the scenario 3 with only 2 raingauges in Event 1 and the scenario 4 with 3 raingauges in Event 2 optimally present the actual spatiotemporal variability of rainfall.

In the context of equifinality, indistinguishable runoff simulation in spite of poor consideration of spatial variability rainfall, we can be concerned about the following questions.

1) How internal responses of catchment whatever they are react to plausible rainfall data containing very similar information regarding the total amount and temporal variability (*e.g.* scenario 3 and 8 in Event 1; scenario 4 and 8 in Event 2)?
2) If unlike reproduced hydrographs from plausible input sets, the variation of internal responses of a catchment is very sensitive to plausible scenarios, how can we demonstrate the difference between modeled results?
3) How significant is scale effect in terms of topographic spatial resolution on internal responses of a catchment?

To account for the influence of plausible input data on interior catchment responses, we adopt the computational tracer method developed by Sayama *et al*. (2007). This method is useful and effective to trace the spatiotemporal origins of simulated hydrographs without any hydrochemical measures for a catchment scale. We present the spatiotemporal variation of flow pathways as comparing results between original input based on scenario 1 of both events and plausible inputs, scenarios 3 and 8 for Event 1 and scenarios 4 and 8 for Event 2. The comparison results also may provide helpful information to solve geochemical problems in distributed environmental modeling regarding pollutant transport and acidification of groundwater and so on.

4.3 Effect of input uncertainty on internal responses of catchment.

4.3.1 Comparison of spatial origin of streamflow between original and plausible rainfall data

The Kamishiiba catchment is represented by 3490 and 860 slope elements for 250m and 500m DEMs respectively, as shown in Figure 2 (*i.e.* ***S***=3,401 and 860 for 250m and 500m DEMs). Each slope element contains the information of spatial origins of streamflow for every 1hr time step of two events. The degree of contribution of each slope element to runoff generation at the specific time step of interest is represented by Relative Ratio of Total Discharge (RRTD), defined as:

$$\begin{aligned} &\mathrm{RRTD}_i(t) = \frac{D_i(t)}{D^{outlet}(t)} \times 100 \quad (\%) \\ &\sum_{i=1}^{S} \mathrm{RRTD}_i(t) = 100 \quad (\%) \end{aligned} \tag{10}$$

where i is slope number and $D_i(t)$ is runoff from slope element i to the outlet at time t. $D^{outlet}(t)$ is the hydrograph ordinate of the outlet at time t. Four particular time steps, 1, 12, 36 and 72 hours for Event 1 and 1, 72, 132 and 168hours for Event 2 are selected, respectively in order to visualize the spatial origins of the runoff for two historical events and compare those from plausible rainfall scenarios to the results based on scenario 1, original radar rainfall data. Each RRTD for four chosen time steps is categorized into seven classes as shown in Figures 10 and 11. Colorful snapshots for spatially distributed origin apparently present that even though global responses of catchment with respect to the plausible rainfall patterns are nearly identical, the internal responses are completely different according to the spatial patterns of rainfall.

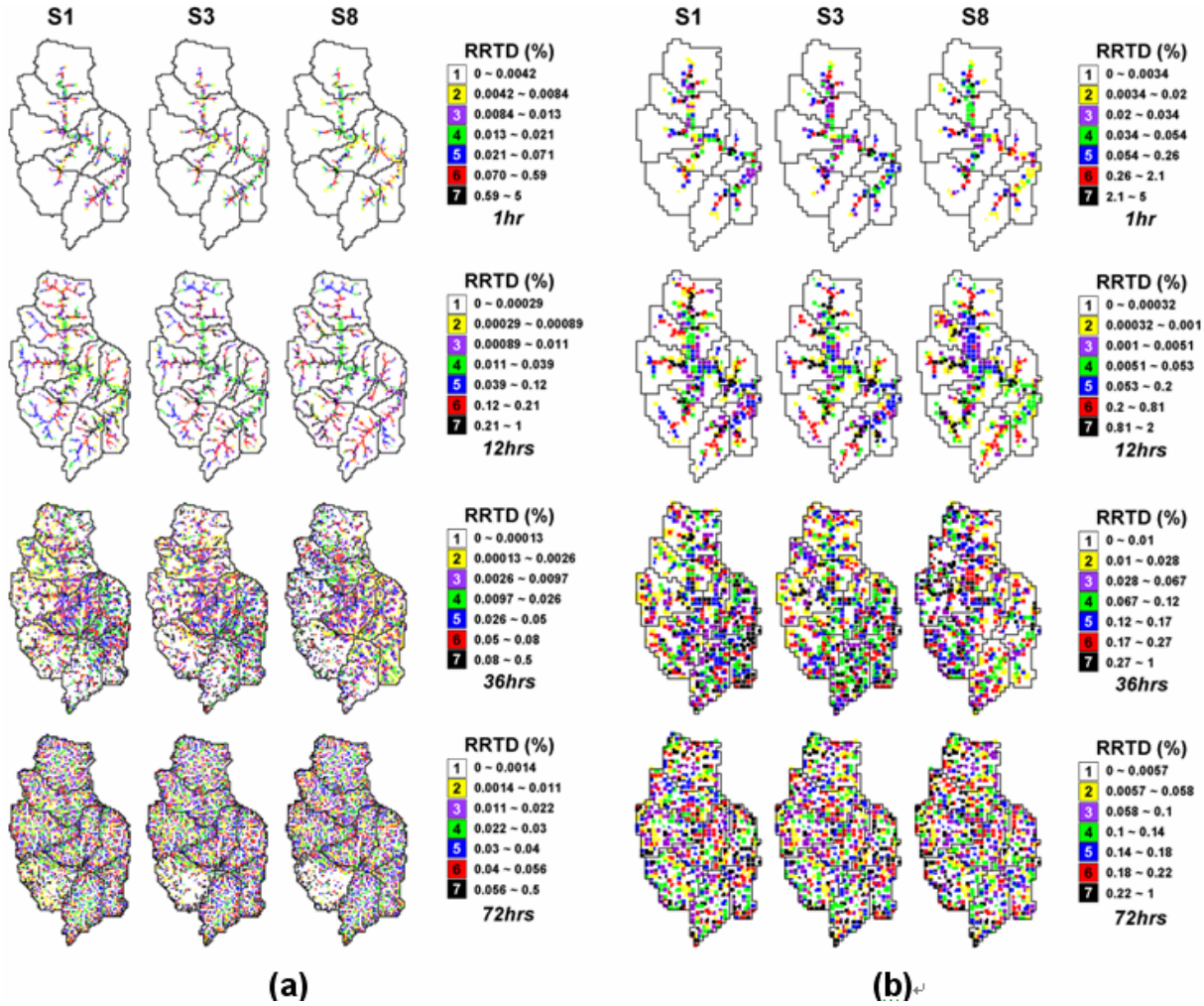

Fig. 10 Effect of input uncertainty due to spatial variability of rainfall on internal catchment response, spatially distributed origins of streamflow for scenario 1, 3 and 8 in Event 1; (a) 250m-based and (b) 500m-based result.

At the beginning of rainfall-runoff process (*e.g.* 1hour), the adjacent slope elements to river channel, referred to as riparian zone constitute primarily the streamflow while water stored in upstream slope elements still do not reach the river channel. As time goes on, contributive slope elements spread gradually across the catchment and eventually, all of slope elements influence streamflow generation. How much each slope element contributes to generate streamflow at each time step is quantified by simple index, Contributing Percentage of sub-catchment (CP), expressed as:

$$\begin{aligned} &\mathrm{CP}_j(t) = \sum_{i \in j} \mathrm{RRTD}_j(t) \\ &\sum_{j=1}^{8} \mathrm{CP}_j(t) = 100 \quad (\%) \end{aligned} \tag{11}$$

where j is sub-catchment number; the study catchment is divided into 8 sub-catchments to compare the variation of contributing area due to plausible rainfall scenarios. The variations of CPs for applied scenarios, summarized in Figure 12 (Event 1) and 13 (Event 2), show that the spatial pattern of plausible rainfall scenarios leads to the significant predictive uncertainty of internal catchment response despite their equivalent runoff.

At 1hour time step of both events, the patterns of contributing sub-catchment are too much different while the patterns of scenario 1 and 3 in Event 1 and of scenarios 1 and 4 in Event 2 show similar trends of the runoff generation as the catchment is saturated during events. However, the results for scenario 8 shows the opposite drifts to original rainfall fields of scenario 1 because of the orderly rearranged rainfall cells while the discrepancy of contributing patterns to scenario 1

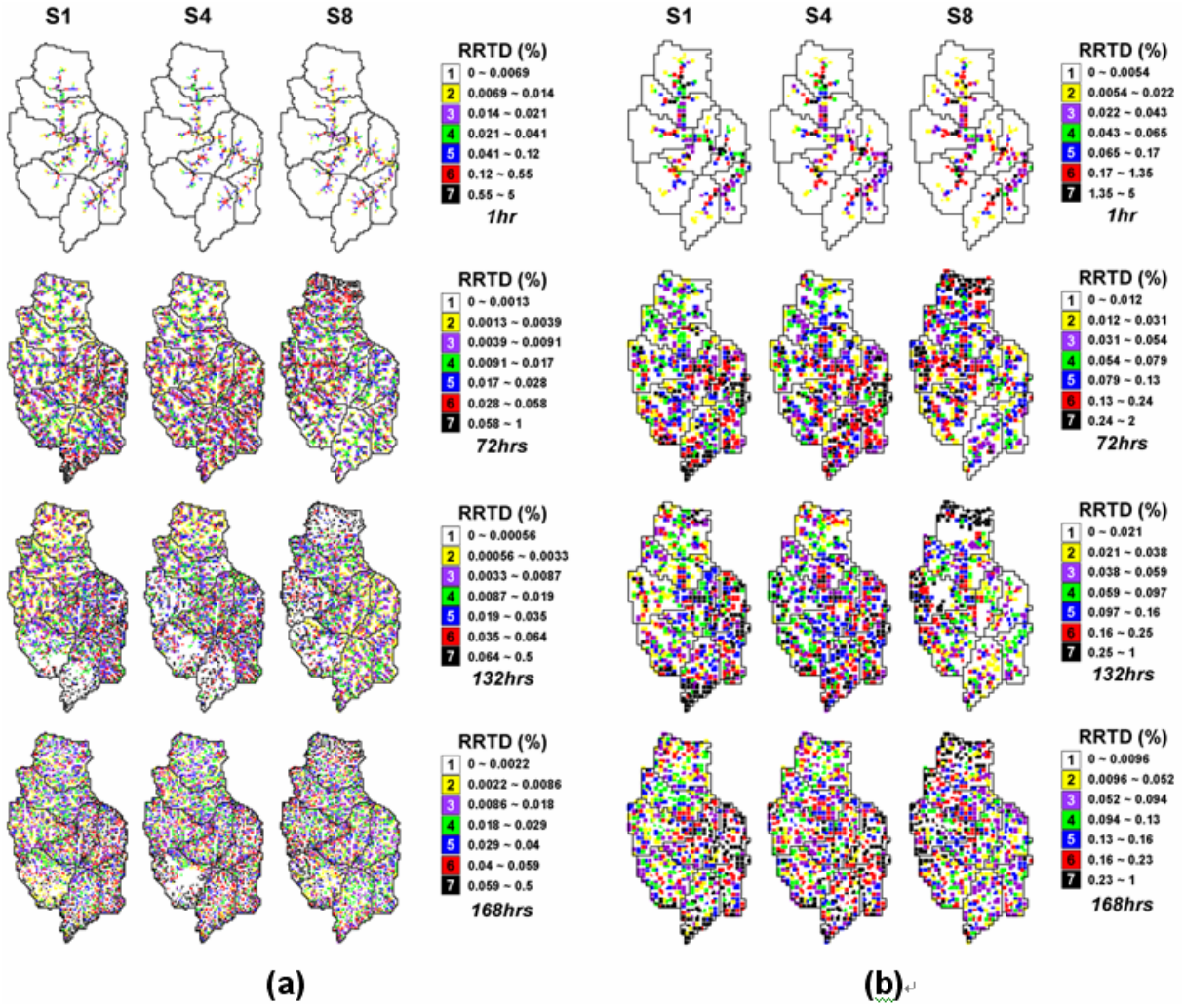

Fig. 11 Effect of input uncertainty due to spatial variability of rainfall on internal catchment response, spatially distributed origins of streamflow for scenario 1, 4 and 8 in Event 2; (a) 250m-based and (b) 500m-based results.

becomes narrower during non-storm periods such as 72hours in Event 1 and 168hours in Event 2 (*i.e.* after stopping rainfall). Moreover, the effect of topographic resolutions on the distribution of spatial origin is not considerable since the volume of rainfall falling on each sub-catchment is not different significantly for the applied DEM sizes.

From these results, it can be seen that a distributed rainfall-runoff model can allow multiple alternative flow pathways, yielding very similar hydrographs, due to the spatial variability of rainfall even though the modeling is conducted based on the single optimal parameter set. In other words, it means that the effect of difference in spatial pattern of rainfall is smoothen and attenuated as a result of the diffusive redistribution of water when the rainfall over the catchment drains into the downstream outlet in form of either surface /subsurface flow or a mixture of both.

4.3.2 Comparison of temporal origin of streamflow between original and plausible rainfall data

The historical two events are split into six temporal classes (*i.e.*, ***T***=6: pre-event, 0~15hrs, 16~22hrs, 23~30hrs, 31~34hrs and 35~84hrs in Event 1; pre-event, 0~24hrs, 25~95hrs, 96~108hrs, 109~119hrs and 120~192hrs in Event 2) and then the simulated hydrographs based on scenario 1 and plausible scenarios are separated into six corresponding runoff components to each rainfall duration by using spatiotemporal matrix of streamflow records.

Figure 14 presents the results based on 250m and 500m DEMs under the original and plausible scenarios, temporally separated hydrographs with respect to selected rainfall durations for the two events. The volume of pre-event water for 500m DEM-based modeling is similar as those of 250m DEM-based result for both events. It implies that even if the density

of drainage network is different due to different spatial resolution of DEM, temporal variation of internal responses of catchment is quite similar since both amount of rainfall depth over the catchment and corresponding best-performing parameters to each resolution provide the equivalent results. This result would be very important for distributed environmental models related with groundwater-induced pollutant release or transport, which are in need of antecedent soil condition of a catchment.

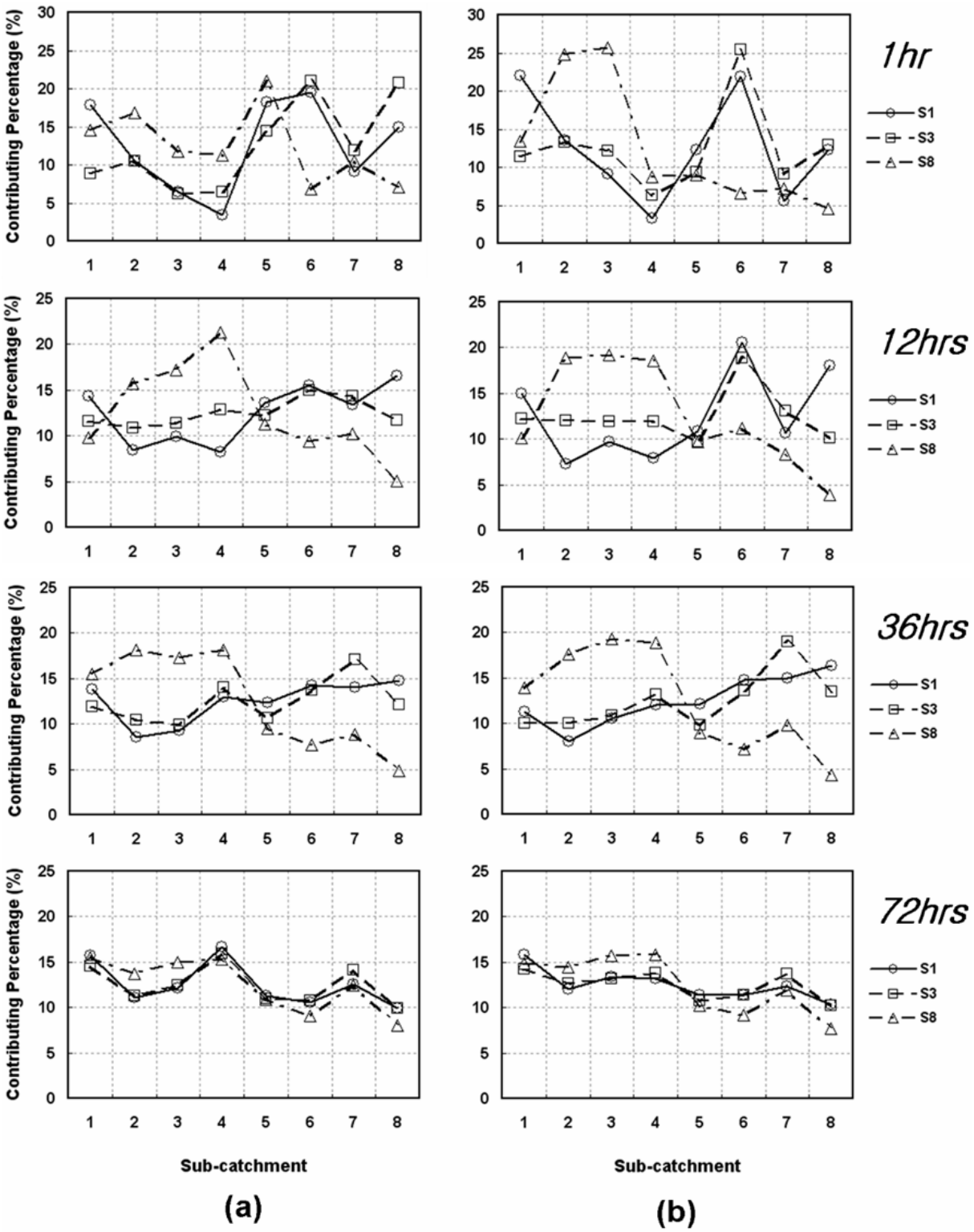

Fig. 12 Variation of the Contributing Percentage (CP) of each sub-catchment due to mimic rainfall scenarios for Event 1; (a) 250m-based and (b) 500m-based results.

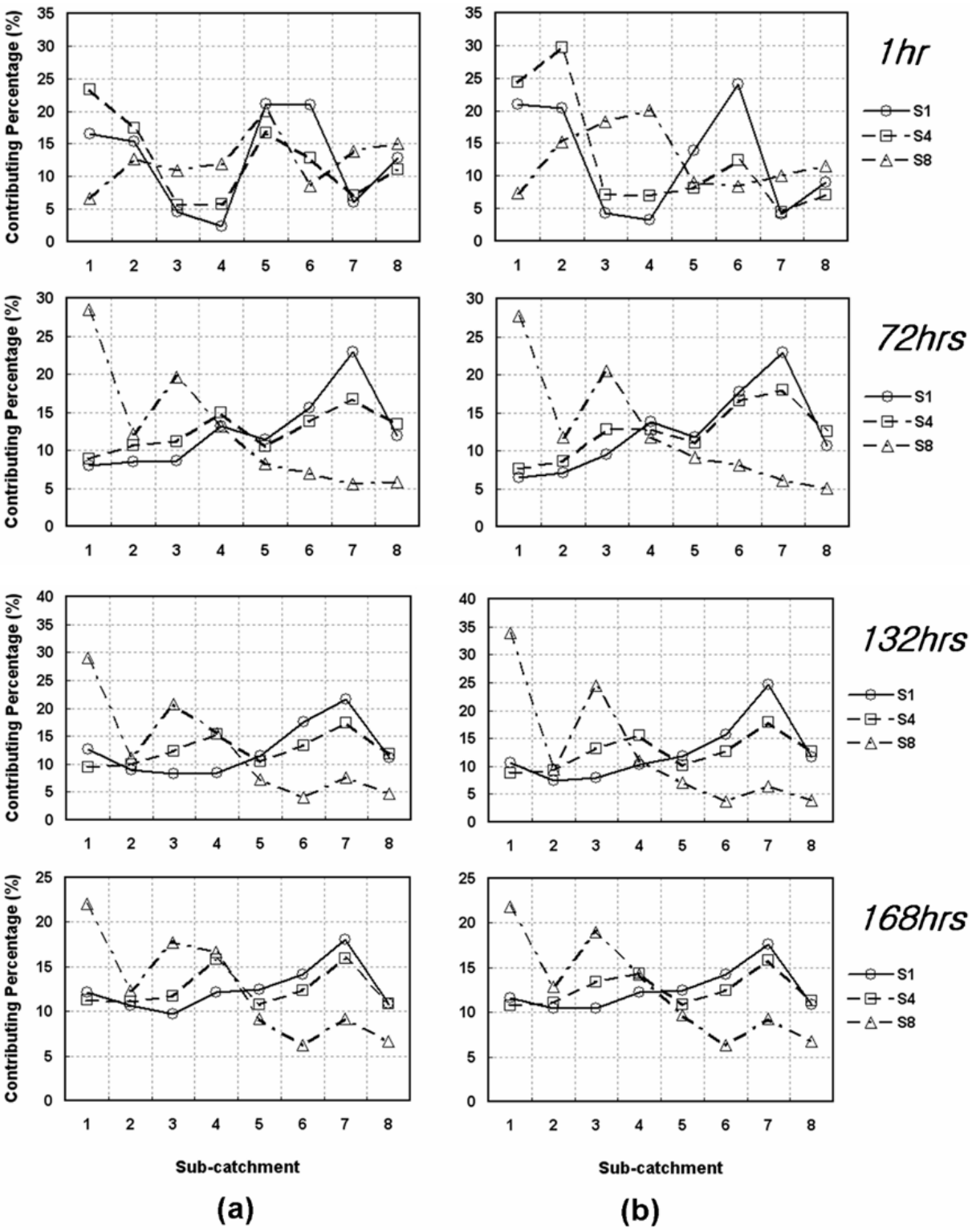

Fig. 13 Variation of the Contributing Percentage (CP) of each sub-catchment due to mimic rainfall scenarios for Event 2; (a) 250m-based and (b) 500m-based results.

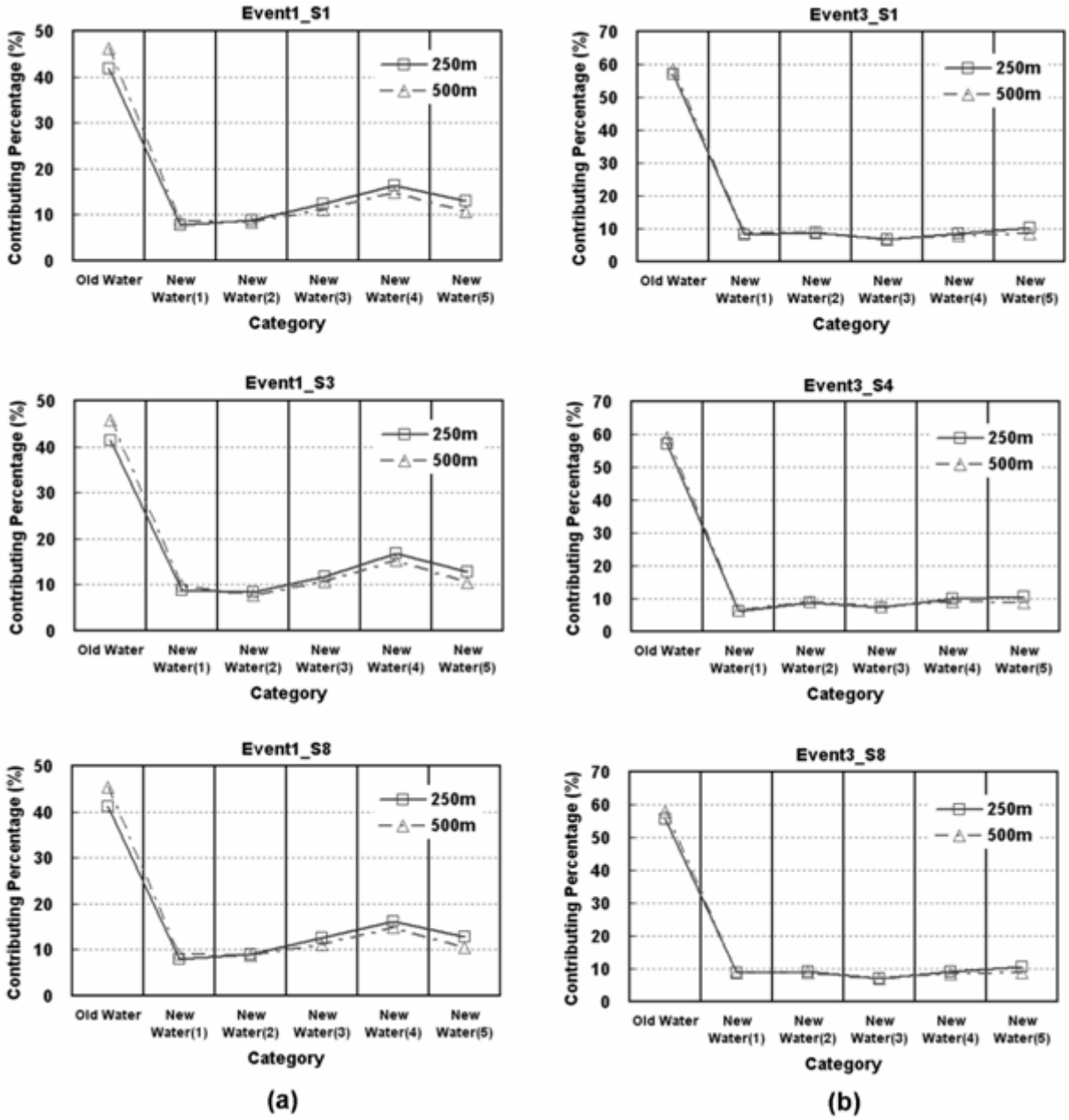

Fig. 14 Corresponding variation of the Contributing Percentage (CP) to each rainfall duration selected under scale dependent condition with three rainfall scenarios; (a) Event 1 and (b) Event 2.

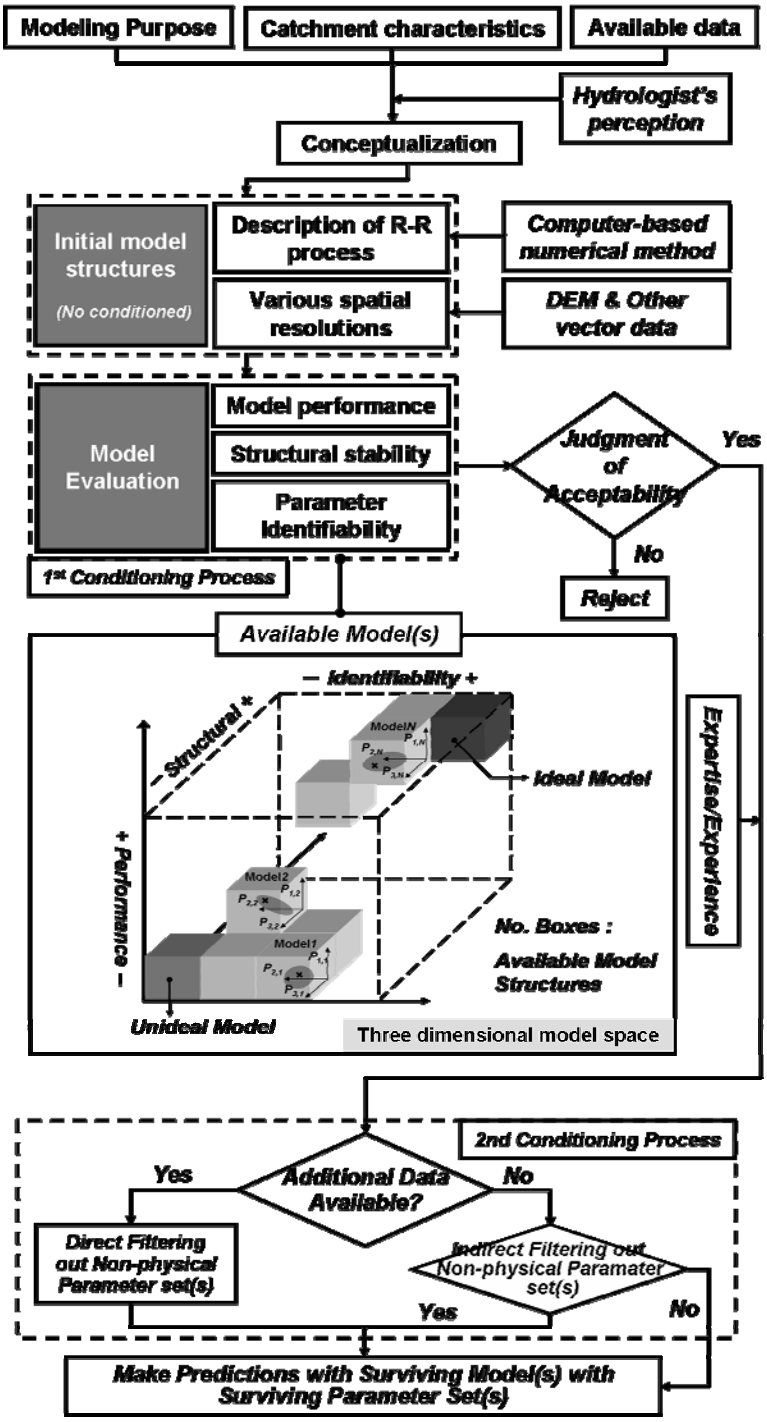

Fig. 15 Schematic stepwise procedures of the newly proposed modeling framework.

5. Extended Rainfall-Runoff Modeling Framework under Uncertainty

Figure 15 presents the extended modeling framework considering uncertainty which consists of two conditioning processes in order to narrow down reliable model structures and their corresponding parameter sets.

Initially, a set of model structures, ranging from simple lumped bucket model to scale-dependant distributed models (refer to section 2.1) is prepared to analyze the influence of model complexity on performance and prediction uncertainty. All initial model structures are developed under Object-oriented Hydrological Modeling System, OHyMoS (Takasao *et al*., 1996, Ichikawa *et al*., 2000). It is assumed that initial model structures can be potential simulators, until there appears an obvious evidence to reject it.

One should then apply three evaluative criteria to the competing models. It means that under-performing structures can be rejected at this stage, based on the each evaluative criterion value. First measure of model evaluation is a model performance index (MPI), which allows to assessing whether or not the model is capable of accurately simulating a hydrological behavior. The second is a model structural stability index (MSSI) in order to assess the suitability of process description underlying the model's structure for the various response modes (*e.g.*, low and high flow period within single event or different climatic conditions). Last measure is a model parameter identifiability index (MPII) capable of assessing whether or not the model parameters are well identified within predefined parameter feasible space. As a consequence, the estimated values in different ways form the basis of a knowledge-based guide to confirm or reject model structure(s).

However, even the best balanced model structure still suffers from equifinality problem. Plausible parameter combinations (*i.e.*, light grey shaded elliptical region of feasible parameter space in Figure 15; $P_{i,j}$ is a model parameter where *i* is the number of parameter to be calibrated and *j* is the number of possible model structure) that yield similarly good outcomes, as well as those obtained by global optima (*i.e.*, ex marks on parameter space of each model), are widely distributed in parameter space so that it is essential to impose additional constraints on the calibrated model for filtering out non-physical parameter sets.

If we have additional observed data sufficiently, which are apart from streamflow data, this auxiliary constraint in terms of the second conditioning process is meaningful to directly reject unreliable parameter combinations. In spite of efficiency of complementary data, many of catchment do not have enough additional measured data. In line with practical way, an indirect filtering approach based on hydrologists' expertise can be an alternative constraint, but still be likely to receive criticism because of its subjectivity. However, it is sure that the complementary information containing physics-based meaning is necessary for further rejection or corroboration, irrespective of whether it is measurable or not.

Finally, surviving model(s) with behavior parameter set(s) should be retained unless and until they violate new evaluative criteria and then used to make prediction of catchment response. In other words, prediction result of the new modeling framework under uncertainty is not a single output time series but an ensemble prediction of the system behavior.

The above mentioned simple bucket model (*i.e.*, SFM) and kinemtic wave models (*i.e.*, KWMSS1 and KWMSS2) with three different DEMs, 250m, 500m and 1km are evaluated under this new modeling framework.

5.1 Model evaluation; First conditioning process

The purpose of model evaluation is fundamentally to understand characteristics of each model structure and establish preferences between competing model structures in regard of three different criteria, model performance, parameter identifiability and structural stability. An ideal model may have a perfect model structure (*i.e.*, the most appropriate representation of natural hydrological system), and then provide an accurate prediction results. In addition, its response surface of parameter may be very convex or concave so that global optimum can be easily found out using efficient automatic optimization algorithms. One dimensional model space (Beven, 2002) based on only model performance is replaced by three dimensional one in order to provide a more extensive guideline with respect to selecting an adequate model structure.

5.1.1 Model Performance Index (MPI)

In this study, the hydrograph is simply partitioned into two components; high and low flow period separated by mean value of observed discharge data. The performance of each model structure is assessed using NSC value for two periods and the average of two measures is referred to as the MPI, defined as:

$$\mathrm{MPI} = 0.5(\mathrm{NSC}_{High} + \mathrm{NSC}_{Low}) \tag{12}$$

$$\mathrm{NSC}_{\mathrm{High}} = 1 - \frac{\sum_{t=1}^{N_{High}} (q_{obs}(t) - q_{sim}(t))^2}{\sum_{t=1}^{N_{high}} (q_{obs}(t) - \overline{q}_{obs}^{High})^2} \tag{13}$$

Table 1. MPI for each model structure

Model / Value	SFM	KWMSS1			KWMSS2		
		250m	500m	1km	250m	500m	1km
NSE_{Low}	0.944	0.885	0.885	0.812	0.993	0.993	0.974
NSE_{High}	0.987	0.969	0.969	0.967	0.993	0.992	0.983
MPI	0.977	0.95	0.95	0.931	0.993	0.993	0.981

$$\mathrm{NSC}_{\mathrm{Low}} = 1 - \frac{\sum_{t=1}^{N_{Low}} (q_{obs}(t) - q_{sim}(t))^2}{\sum_{t=1}^{N_{Low}} (q_{obs}(t) - \overline{q}_{obs}^{Low})^2} \qquad (14)$$

where $q_{obs}(t)$ is the observed discharge at time step *t*, $q_{sim}(t)$ the simulated discharge, $\overline{q}_{obs}^{High}$, $\overline{q}_{obs}^{Low}$ the mean observed discharge over the simulation periods of length, N_{High}, N_{Low}.

A flood event with short duration (84hr) is designated for calibration of each model and parameters of all testable model structures are tuned using SCE-UA algorithm with SLS (see Eq.(6)). Evaluation of model performance is quantified by the MPI value as summarized in Table 1.

This table shows that all models yield acceptable values quantitatively. In particular, KWMSS1 provides a good agreement during high flow period while it cannot reproduce accurately rising and recession limbs of hydrograph. It means that its underlying assumption of model structure is not proper to simulate the low flow so that it is in need of further modification. On the other hand, both SFM and KWSSM2 reproduce relatively balanced hydrographs even if the simulated recession part of SFM is slightly underestimated. It supports the fact that the hydrologists, if armed with sufficient data in terms of quality and quantity, do not need to choose a complicated hydrologic model for simulating streamflow because it does not lead to significant improvements (Jakeman and Hornberger, 1993).

5.1.2 Model Structural Stability Index (MSSI)

Structure error is unavoidable problem in hydrological modeling since a hydrologic model is conversion and simplification of reality, thus no matter how sophisticated and accurate they may be those models only represent aspects of conceptualization or empiricism of modelers. In consequence, output time series of hydrologic models are as reliable as hypothesis, structure of models, quantity and quality of available forcing data, parameter estimates. Gupta *et al*. (1998) demonstrated that one parameter set might be insufficient to represent the entire behavior of the catchment due to the inadequacy of model structures. In other words, a subjective selection of objective functions for calibration of conceptual hydrologic models results in an overemphasis on different response modes such as low and high flow period. In this regard, the result of variation of optimal parameter combination calibrated by a single-objective optimization method can be used as one of the well-founded indicators to account for model structural stability (Lee *et al*., 2007). Moreover, such model structures provide relatively acceptable simulated hydrographs when applying parameter set for various type and magnitude of floods within a particular study site. It means that a structurally-stable model has high parameter transferability from event to event. As a result, model structural stability can be estimated as a degree of ability capable of reducing the influence of objective functions and flood events on model parameter sets.

SCE-UA with two different objective functions, the SLS and Heteroscedastic Maximum likelihood Estimator (HMLE, Sorooshian and Dracup, 1980) is used to calibrate each model structure. Note that the several objective functions, conversions of SLS have square terms in their function, thereupon, they are in danger of emphasizing on the similar particular response like high flow. Accordingly, the objective functions having different characteristic should be used for the structural stability analysis. HMLE is formulated as:

$$\mathrm{HMLE} = \frac{1}{N}\sum_{t=1}^{N} w_t (q_{obs}(t) - q_{sim}(t))^2 \Big/ \left[\prod_{t=1}^{N} w_t\right]^{1/N} \qquad (15)$$

Table 2. MSSI for each model structure

Model / Value	SFM	KWMSS1			KWMSS2		
		250m	500m	1km	250m	500m	1km
MSSI	92.21	3.63	49.46	86.59	9.97	12.97	31.47

Table 3. MPII for each model structure

Model / Value	SFM	KWMSS1			KWMSS2		
		250m	500m	1km	250m	500m	1km
MPII	0.103	0.472	0.538	0.402	0.151	0.112	0.429

$$\mathrm{MSSI} = \sqrt{\frac{1}{N}\sum_{t=1}^{N}\left(q_{SLS}(t) - q_{HMLE}(t)\right)^2} \qquad (16)$$

where $w_t = \left(q_{obs}(t)\right)^{2(\lambda-1)}$ is weight, λ is the transformation parameter, N is total number of simulation time step, $q_{SLS}(t)$ and $q_{HMLE}(t)$ are the simulated discharges with each optimal parameter set based on SLS and HMLE, respectively. The lower value of MSSI indicates the more stable model structure.

Table 2 shows that there is slight or no influence of objective functions on model performance in the KWMSS2 applications but the finer grid size leads to smaller difference between two reproduced hydrographs. This result implies that the parsimonious models used in this study such as the SFM and the KWMSS1 with coarse resolutions are structurally unstable in terms of dependency of model performances on the objective functions so that we need to change the model parameter set according to the modeling purpose. On the other hand, the problem of subjectivity related with selection of objective functions for the automatic calibration can be ignored in the distributed hydrological modeling using the KWMSS2.

Another interesting finding is that although the sophisticated model structure has high structural stability, the constant parameter set is not obtained for SLS and HMLE. Instead, both parameter combinations provide equally good measures in terms of model performance. The result suggests that increased model complexity in terms of description of rainfall-runoff process leads to increased structural stability while the identifiability of the model parameters decreases. In the subsequent subsection, we discuss in detail the method to assess parameter identifiability.

5.1.3 Model Parameter Identifiability Index (MPII)

In this study, we apply Shuffled Complex Evolution Metropolis (SCEM-UA; Vrugt *et al*., 2003) method to estimate posterior parameter distribution and then the highest density value of each distribution is referred to as the indicator of individual parameter identifiability. The mean of these maiximum identifiability values for each model structure is utilized as MPII. Moreover, we can quantify the uncertainty associated with parameters of the estimated posterior distributions and then it gives the basis for making probabilistic predictions.

SCEM-UA algorithm was implemented with iteration numbers 10000, a population size 200, complexes 10 and 20 points in each complex. The first 4000 simulations of each parallel sequence are referred to as non-behavioral parameter sets and then are discarded. From the remaining 6000 simulations, the prior ranges of each parameter are split into 100 containers and the samples within each bin are counted to calculate the frequencies. Resulting frequencies are transformed into probability density function so that the best performing parameters are assigned the highest value and all measures sum to unity. This highest density function value is utilized as the index for parameter identifiability. Figure 16 and Table 3 present the estimated posterior parameter density and MPII for each model structure.

In distributed modeling, it can be seen that the simpler model structure, KWMSS1 shows generally

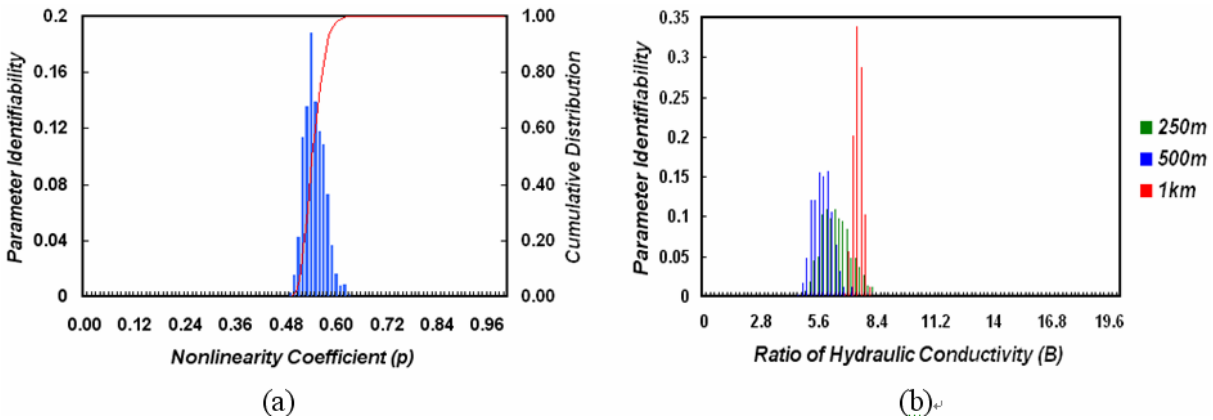

Fig. 16 Estimation of parameter identifiability for (a) p of SFM and (b) β of KWMSS2 based on different DEMs

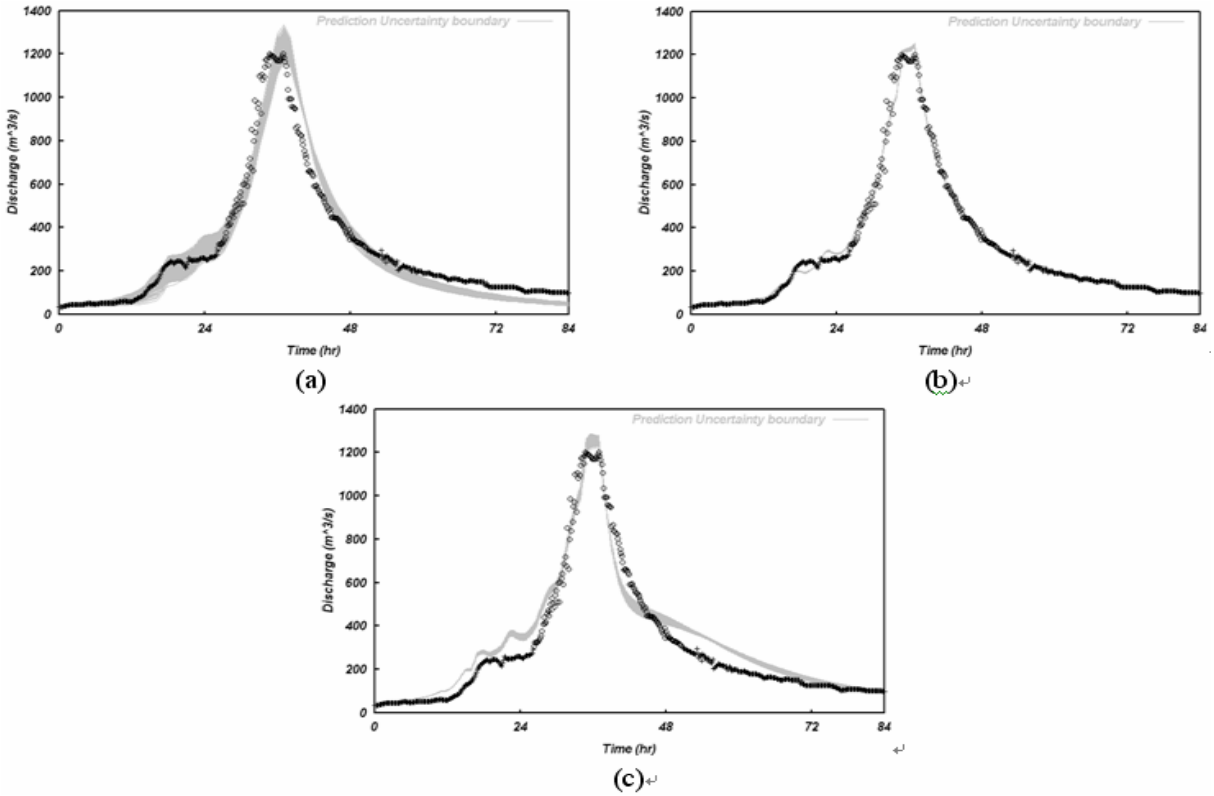

Fig. 17 Hydrograph prediction uncertainty associated with the most probable set derived using the SCEM-UA; (a) SFM, (b) KWMSS2 based on 500m DEM and (c) KWMSS1 based on 500m DEM.

higher MPII than KWMSS2. It is interpreted that parameter interaction of two additional parameters of KWMSS2 with other parameters results in poor identifiability. However, the structurally-simplest model, SFM has the lowest MPII and the coarse DEM-based models sometimes lead to worse identifiability than the fine DEM-based models (*i.e.*, indeed, the 1km-based KWMSS1 shows lower MPII than the 250m and 500m-based ones). It implies that MPII is rather dependant on the level of interaction due to additional parameter than the degree of abstraction with respect to either rainfall-runoff mechanism or topographic representation.

5.2 Parameter filtering; Second conditioning process

Probabilistic predictions of the hydrograph are obtained from the ensemble simulation of poorly

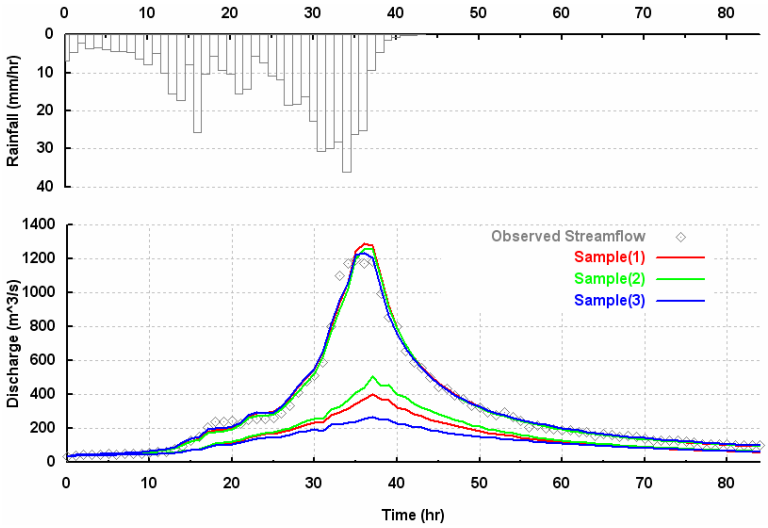

Fig. 18 Separated hydrographs into old water and new water components by three plausible parameter sets.

identified models, SFM and KWMSS2 based on 250m DEM and well identified model, KWMSS1 based on 500m DEM for the behavioral parameter combinations sampled from the each posterior parameter distribution. Figure 17 illustrates how the parameter uncertainty can be translated into estimates of hydrograph prediction uncertainty.

In these figures, the black marks indicate the observed streamflow data and the grey shaded region, 90% hydrograph prediction uncertainty associated with the posterior distribution of the parameter estimates. The parameter uncertainty of SFM results in very wide prediction uncertainty boundary while the simulated hydrographs of KWMSS2 mostly propagate into narrow range like single line. It supports that complex hydrological modeling is likely to be overly exposed to equifinality problem so that it makes difficult to discriminate quantitatively and qualitatively between reliable and unreliable parameter sets. Moreover, prediction boundaries estimated by the posterior distributions of SFM and KWMSS2 fail to bracket the observations for the most period; particularly, the recession part of simulated hydrograph is not matched to the observed one. It means that improvements in model structures or calibration data may result in more accurate predictions when compared with KWMSS2.

5.2.1 Potential use of additional constraint, catchment response

We used the same method described in section 4.3.2 to show how the runoff components, new water and old water, react to plausible parameter sets. They are reproduced by three sample parameter sets containing different values, which are given from 6000 behavioral parameter combinations in KWMSS2 with 500m spatial resolution.

Figure 18 clearly shows that even if overall responses of catchment to these three mimic parameter sets are nearly identical, internal responses to them are too much different according to parameter values. In other words, this information can be potentially used to reject unreliable parameter set. However, we do not have observed data with respect to proposed complementary information. If this methodology is applied to the specific study area with the observed data such as hydrochemical materials including isotope tracers, more reliable parameter sets will be selected.

Because of no comparable data, it is still questionable which parameter is more physically-based among three samples. It means that these plausible sets should be retained for model prediction unless and until additional evidence to the contrary (*e.g.*, actual old water data) becomes apparent because even auxiliary information used here cannot constrain the model completely.

6. Conclusions

This paper aims at investigating prediction uncertainty due to input and parameter under scale-dependant condition of a rainfall-runoff modeling. Moreover, a new rainfall-runoff modeling

framework considering uncertainty components involved in modeling processes is proposed to provide guideline for future modeling direction. The results obtained in this study can be summarized as follows:

1) Parameter compatibility is evaluated for both improving computational efficiency of distributed rainfall-runoff modeling with very fine resolution and exemplifying 'equifinality' problem arising from a complex drainage network derived from small spatial resolution of DEM.
2) The model based on fine spatial resolution has good parameter compatibility but high potentiality of equifinality problem
3) Scenario-based applications are performed to examine the effect of input uncertainty due to spatial variability of rainfall data on model predictions.
4) Plausible rainfall scenarios result in equally good hydrographs but internal responses to them show too much different aspects
5) Three guideline indices with respect to model performance, structural stability and parameter identifiablity are proposed to explain limitations of a conventional modeling protocol and then new modeling framework is developed by incorporating these indices into model evaluation procedure.

In further study, we apply the proposed new modeling framework to the area having abundant observed data including streamflow and other hydrological variables in order to verify it and to articulate the need of alternative direction toward model testing in hydrology.

References

Beven, K. and Hornberger, G.M. (1982): Assessing the effect of spatial pattern of precipitation in modeling streamflow hydrographs, *Water Resources Bulletin*, 18(5), pp. 823-829.

Beven, K., and Binley, A.M. (1992): The future of distributed models: model calibration and uncertainty prediction, *Hydrol. Processes*, 6(3), pp. 279-298.

Beven, K. (2002): Towards an alternative blueprint for a physically-based digitally simulated hydrologic response modeling system, *Hydrol. Processes*, 16(2), pp. 189-206.

Duan, Q., Sorooshian, S. and Gupta, V.K. (1992): Effective and efficient global optimization for conceptual rainfall-runoff models, *Water Resour. Res.*, 28(4), pp. 1015-1031.

Franks, S.W., Uhlenbrook, S. and Etchevers, P. (2006): Hydrological simulation, in *Hydrology 2020: An integrating Science to Meet World Water Challenges*, edited by T. Oki, Valeo, C. and Heal, K., pp. 105-122, *IAHS Press*, Wallingford.

Gupta, H.V., Sorooshian, S. and Yapo, P.O. (1998): Toward improved calibration of hydrological models: Multiple and noncommensurable measures of information, *Water Resour. Res*., 34(4), pp. 751-763.

Gupta, H.V., Sorooshian, S., Hogue, T.S. and Boyle, D.P. (2003): Advances in automatic calibration of watershed models, in *Advances in calibration of watershed models*, pp. 29-47, edited by Q. Duan, S. Sorooshian, H.V. Gupta, A. Rosseau, R. Turcotte, *AGU*, Washington, D.C..

Ichikawa, Y., Shiiba, M., Tachikawa, Y. and Takara, K. (2000): Object-oriented hydrological modeling system, *Proc. of 4th International Conference Hydro informatics 2000* CD-ROM, Iowa, USA.

Jakeman, A.J. and Hornberger, G.M. (1993): How much complexity is warranted in a rainfall-runoff model?, *Water Resour. Res.*, 29(8), pp. 2637-2649.

Lee, G., Tachikawa, Y. and Takara, K. (2006): Analysis of Hydrologic Model Parameter Characteristics Using Automatic Global Optimization Method, *Annuals of Disaster Prevention Research Institute*, Kyoto Univ., No. 49B, pp. 67-81.

Lee, G., Tachikawa, Y. and Takara, K. (2007): Identification of model structural stability through comparison of hydrologic models, *Annual J. Hydraul. Eng.*, JSCE, 51, pp. 49-54.

Lee, G., Tachikawa, Y., Sayama, T. and Takara, K. (2008): Internal response of catchment to plausible parameter sets under equifinality, *Annual J. Hydraul. Eng.*, JSCE, 52, pp. 79-84.

Melching, C.S. (1995): Reliability estimation, in *Computer models of watershed hydrology*, edited by Singh , V.P., pp. 69-118, *Water Resources Publications*, Highland Ranch.

Obled, Ch., Wendling, J. and Beven, K. (1994): The sensibility of hydrological models to spatial rainfall patterns: an evaluation using observed data, *Journal of Hydrology*, 159, pp. 305-333.

Sayama, T., Tatsumi, K., Tachikawa, Y. and Takara K. (2007): Hydrograph separation based on spatiotemporal record of streamflow in a distributed

rainfall-runoff model, *J. Japan Society of Hydrol. & Water Resours.*, JSCE, 20(3), pp. 214-225 (in Japanese).

Sorooshian, S. and Dracup, J.A. (1980): Stochastic parameter estimation procedures for hydrologic rainfall-runoff models: Corrolated and heteroscedastic error cases, *Water Resours. Res*., 16(2), pp. 430-442.

Tachikawa, Y., Nagatani, G. and Takara K. (2004): Development of stage-discharge relationship equation incorporating saturated–unsaturated flow mechanism, *Annual J. Hydraul. Eng*., JSCE, 48, pp. 7-12. (in Japanese)

Takasao, T. and Shiiba, M. (1988): Incorporation of the effect of concentration of flow into the kinematic wave equations and its applications to runoff system lumping, *Journal of Hydrology*, 102, pp. 301-322.

Takasao, T., Shiiba, M. and Ichikawa, Y. (1996): A runoff simulation with structural hydrological modeling system, *Journal of Hydroscience and Hydraulic Engineering*, JSCE, 14(2), 47-55.

Vieux, B.E. (1993): DEM resampling and smoothing effects on surface runoff modeling. *Journal of Computing in Civil Engineering* 7(3), pp. 310-338.

Vrugt J.A., Gupta, H.V., Bouten, W. and Sorooshian, S. (2003): A shuffled complex evolution metropolis algorithm for optimization and uncertainty assessment of hydrologic model parameters, *Water Resour. Res.*, 39(8), 1201, doi:10.1029/2002WR001642.

Wagener, T. and Gupta H.V. (2005): Model identification for hydrological forecasting under uncertainty, *Stoch. Environ. Res. Risk Assess*, 19, pp. 378-387.

降雨流出モデリングにおける空間スケール依存性のもとでの水文予測の不確実性の評価

Giha LEE*・立川康人*・宝　馨

＊京都大学大学院工学研究科 都市環境工学専攻

要　旨

本研究では，降雨流出モデリングにおけるスケール依存性のもとでのモデルパラメータと入力に起因する水文予測の不確実性を分析することを目的とする。さらに，水文モデリングにおけるガイドラインを提供するために，水文モデリングの過程で含まれる不確かさの要素を考慮した新しい降雨流出モデルの枠組みを示す。まず，分布型流出モデルの構成に用いる数値標高モデルの適切な分解能を定めるためにモデルパラメータの適応性を評価する。次に，降雨の空間分布による入力の不確かさが流出予測に及ぼす影響を分析する。最後に，水文モデルの予測性能，モデル構造の安定性，パラメータの唯一決定性に関して３つの指標を提案する。これによって，従来の水文モデリングの限界を説明することが可能となる。また，これらの３つの指標をモデル評価の手順に導入した新しい水文モデルの枠組みを提案する。

キーワード：予測の不確かさ，パラメータの適合性，降雨の空間分布，新たなモデル化の枠組み